IBFD for seismic wave modeling -A regular grid method handling arbitrary topography

Wenyi Hu, Advanced Geophysical Technology Inc.*

Summary

To accurately simulate seismic wave propagation for the purpose of land data acquisition, processing, and interpretation, especially for land data full waveform inversion (FWI), we developed an efficient high-order finite-difference modeling algorithm with the capability of handling arbitrarily shaped surface topography. Unlike most of the existing modeling algorithms dealing with irregular surface topography, this finite-difference algorithm, based on an immersed boundary (IB) method, uses regular Cartesian staggered or collocated grid system without suffering from the well-known staircasing error. In this immersed boundary finite-difference (IBFD) algorithm, arbitrary surface topography is accounted for by imposing the free surface boundary conditions at the exact boundary locations instead of using body-conforming grids, thus greatly reducing the complexity of preprocessing procedures. Furthermore, local continuity and curvatures (including sub-cell curvatures) are represented precisely through the employment of a local cylindrical or a spherical coordinate system. Wavefield values in a ghost zone required for boundary condition enforcement are obtained using a special recursive interpolation technique, which simplifies the boundary treatment and further improves the accuracy, as validated by the numerical simulation. Another unique feature of this algorithm is that the stencil length for ghost zone wavefield interpolation is adaptively determined by the local curvature to maintain the accuracy and stability. This method is a general algorithm applicable to acoustic, elastic, 2D, 3D, and anisotropic cases. A numerical example is presented to show its excellent performances compared with the conventional finite-difference method.

Introduction

Full waveform inversion (FWI) method developed rapidly in recent years because it is regarded as a powerful tool for subsurface structure and property reconstruction. Because it utilizes the full waveform information contained in recorded seismic data, FWI is able to provide high resolution velocity model and other geophysical property models such as anisotropic parameters, attenuation, density, and etc. Unlike conventional processing tools such as velocity tomography using traveltime information only, FWI is mainly based on amplitude fitting between simulated seismic data and recorded seismic data. Consequently, a highly accurate forward modeling engine is necessary for successful FWI inversions. Topography has a significant effect on recorded seismic data. Unfortunately, most existing FWI algorithms use a finite-difference based forward modeling engine and don't have the capability of accurate representation of irregular surface topography. When grid lines of conventional finite-difference methods and free surface boundary are not conformal, staircasing error will be induced, observed as artificial scattering phenomena in the forward modeling results, and severely contaminate the FWI results.

A straightforward conventional finite-difference method for free surface modeling is the so-called image method (Levander 1988; Robertsson, 1996). However, this method is accurate only for flat free surface. For irregular surface topography, grid refinement is necessary near the surface boundary, thus increasing the computational cost dramatically. One category of approaches to circumvent this difficulty uses finite element methods (FEM) (Min et al., 2003) or spectral element methods (SEM) (Komatitsch and Vilotte, 1998), where grid lines are conformal to irregular surface. However, computational cost of FEM can be prohibitive, while the preprocessing procedure, mesh generation, is not a trivial task for SEM. Another category of approaches addressing surface topography adopts a transformation between a curvilinear coordinate system and a Cartesian coordinate system (Hestholm and Ruud, 1998; Appelo and Petersson, 2009; de la Puente et al., 2014). These approaches work only for some cases with simple topography geometry. For topography with high level of irregularity, stability, accuracy, and computational cost can all be serious issues for these methods.

In this work, we developed a finite-difference algorithm, referred to as the immersed boundary finite-difference method (IBFD) for seismic wave propagation simulations with arbitrarily shaped surface topography in presence. The distinguishing feature of the immersed boundary method is that a regular Cartesian grid is employed and the grid lines are not required to conform to the surface boundary. Instead, the surface boundary can cut through the grids and a special interpolation based procedure is carried out to impose the free surface boundary conditions at the exact surface locations. Since the immersed boundary method was first developed by Peskin (1972), many variants of this method have been proposed to address various issues. It has also been introduced to exploration geophysics (Zhang and Symes, 1998; Lombard et al., 2008; Li et al., 2014). We improved this method by introducing some unique technique. Our algorithm differentiates from the above mentioned methods in the following aspects: 1) The local continuity and sub-cell curvature are captured through a local cylindrical or spherical coordinate transformation and this procedure is very straightforward to implement; 2) a special recursive interpolation scheme is used for wavefield

value estimation in ghost zones for artificial scattering artifacts removal; 3) our algorithm is applicable to both standard staggered Cartesian grid and collocated grid system; 4) stencil lengths for ghost zone wavefield interpolation are adaptively determined by the algorithm, allowing one to treat fine geometry features (overhanging structures, thin plates, etc.) accurately; 5) no linear system needs to be solved for ghost zone wavefield estimation, thus avoiding the singularity issue in a matrix inversion.

Conventional Finite-Difference vs. IBFD Method

The acoustic wave propagation equations are as follows:

$$\nabla p + j\omega\rho\mathbf{v} = \mathbf{f}$$
$$\nabla\cdot\mathbf{v} + \frac{j\omega}{\lambda}p = q \qquad (1)$$

where p is the pressure, $\mathbf{v}$ is the particle velocity, ρ is the mass density, $\mathbf{f}$ is the volume density of the body force, q is the volume density of mass, and λ is the bulk modulus. Without losing generality, we use 2-D case as an example.

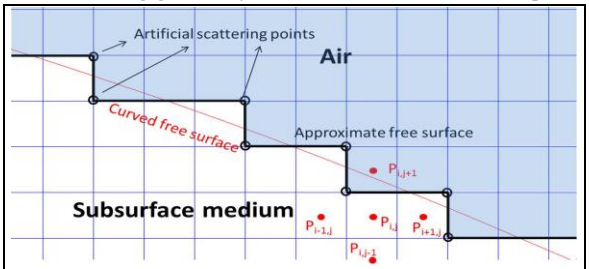

Figure 1: Curved free surface (red curve) and the staircasing free surface approximated by Cartesian grids lines (black lines).

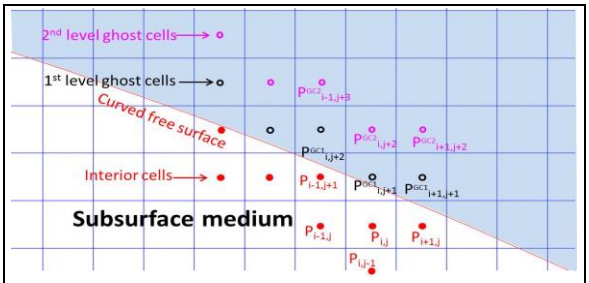

Figure 2:Digram of the grid system of IBFD handling arbitrarily curved free surface topography. Red dots represent the interior cells; black circles represent the 1st level ghost cells; and magenda circles represent the 2nd level ghost cells.

One of the conventional finite-difference methods is the vacuum method, where the curved smooth surface boundary is approximated by a staircasing boundary consisting of Cartesian grid lines, as shown in Figure 1. In the vacuum method, the wavefields in the whole computational domain are updated simultaneously in the same manner. However, the material properties are defined differently. Above the approximate staircasing surface boundary, the mass density is set to a very small value. This method is simple to implement and its physical meaning is clear. Unfortunately, unless extremely small grid size (~60 grid points per wavelength) is used, the artificial scattering points (see Figure 1) will cause the so-called staircasing error and may severely deteriorate the simulation results. This effect will be shown in the numerical simulation results.

Immersed boundary finite-difference (IBFD) offers a simple approach to an accurate representation of arbitrary surface topography under a regular Cartesian grid system. Figure 2 is a diagram of the IBFD grid system, where the regular Cartesian cells are classified into several categories: interior cells, 1st level ghost cells, and 2nd level ghost cells, and so on. Note there is no approximate staircasing surface boundary requried. The true surface boundary is allowed to cut through the Cartesian grids. Furthermore, the material property above the true surface boundary is no longer defined as air. Instead, the stress free (p=0) boundary condition on the true curved free surface is imposed directly by estimating the wavefield values in the ghost cells through interpolation. In other words, the wavefields in the ghost zone are extrapolated from the interior cells with the constraint that the resulting stress on the exact free surface locations must be 0. By doing this, we decoupled the Cartesian grid lines and the true surface boundary without violating the free surface boundary condition. Apparently, the staircasing error caused by the approximate surface boundary in Figure 1 should disappear and this will be validated by the numerical example. After the wavefields in the ghost zone are obtained, we can update the wavefields in the whole computational domain as the conventional finite-difference method for time marching purpose.

Ray-Casting Ghost Cell Wavefield Extrapolation

In this section, we will discuss the approach of ghost cell wavefield extrapolation. There are numerous methods available for ghost cell wavefield extrapolation. Here we follow the approach proposed by Zhao (2010), the ray-casting extrapolation method shown in Figure 3. Here we first investigate scenario A in Figure 3 as an example to explain how we obtain the wavefield p at the 1st level ghost cell G. To carry out the extrapolation for wavefield p estimation at the ghost point G (i.e., p(G)), we generate a normal line passing the ghost point G and perpendicular to the free surface Γ at an intercept point S. In order to achieve high order accuracy, multiple fictitious points (F1, F2, and F3 in Figure 3) are required to enforce the following surface boundary condition at S:

$$c_0^F\, p(G) + \sum_{i=1}^{N} c_i^F\, p(F_i) = p(S) = 0\,, \qquad (2)$$

where c_i^F is the interpolation coefficients associated with the fictitious points, N is the number of fictitious points. Since the fictitious points are not on grids, the wavefields at these fictitious points are evaluated by interpolation using the wavefields at the auxiliary points as shown in Figure 3.

$$p(F_i) = \sum_{j=1}^{M} c_j^A \, p(A_{ij}), \tag{3}$$

where c_j^A is the interpolation coefficients associated with the auxiliary points, and M is the number of the auxiliary points.

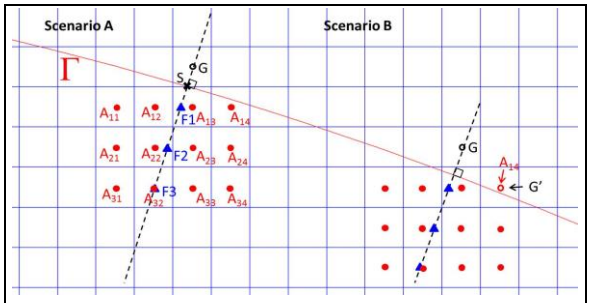

Figure 3: Diagram showing the extrapolation scheme to estimate ghost cell wavefield. Circles are the ghost cells; blue triagles represent the fictitious points; red dots are the auxiliary points.

With (2) and (3), one may obtain the ghost cell wavefield

$$p(G) = -\frac{1}{c_0^F} \sum_{i=1}^{N} c_i^F \sum_{j=1}^{M} c_j^A \, p(A_{ij}). \tag{4}$$

Scenario B is more complicated because one of the auxiliary points is also a ghost point, whose wavefield value is unknown. This phenomenon is common when the curvature is large. We propose a recursive interpolation scheme to address this issue. First, we set all ghost cell wavefields to be 0. Then, we update the ghost cell wavefields one by one using (4) in a recursive manner until convergence is observed. Mathematically, this procedure can be described as

$$\mathbf{P}^{n+1}(G) = \mathbf{C}^A \mathbf{P}(A_{ij}) + \mathbf{C}^G \mathbf{P}^n(G) \tag{5}$$

where $\mathbf{P}^n(G)$ are the wavefields at the ghost cells at the n-th iteration, $\mathbf{P}(A_{ij})$ are the wavefields at the auxiliary points (with those coincident ghost points excluded), and $\mathbf{C}^A$ and $\mathbf{C}^G$ are the corresponding interpolation coefficient matrices. This strategy removes most of the remaining artificial scattering artifacts caused by interpolation errors, which will be shown in the numerical example.

Local Continuity and Sub-cell Curvature Capture

For slowly varying surface geometry, the zero-order stress free Dirichlet boundary condition might be accurate enough to describe the wave propagation behavior. However, for more complex surface topography featuring large curvature, to accurately simulate the rapid wavefield variation near the surface, we may need to impose more strict surface boundary conditions, i.e., the normal and tangential derivative conditions. To enforce these boundary conditions, we introduce a local cylindrical coordinate system (r,φ) as shown in Figure 4.

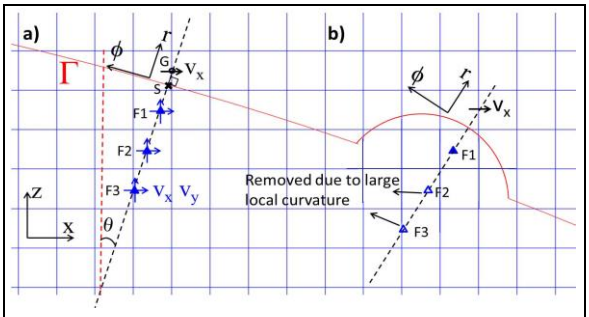

Figure 4: Diagram showing the extrapolation scheme of particle velocity for normal and tangential derivative surface boundary condition enforcement. a) extrapolation scheme and local cylindrical coordinate system; b) adaptive removal of fictitious points for large curvature scenarios.

The normal and tangential derivative boundary conditions under local cylindrical coordinate system can be derived from (1):

$$\begin{cases} v_\phi\big|_\Gamma = 0 \\ \left(\frac{1}{r} v_r + \frac{\partial v_r}{\partial r}\right)\Big|_\Gamma = 0 \end{cases}. \tag{6}$$

Combing (6) and the Cartesian-cylindrical transformation formulation, the particle velocity v_x defined at the ghost point G can be calculated using

$$\begin{aligned} v_x(G) = &-\sum_{i=1}^{N}\left[\frac{\cos^2\theta\, c_i^0}{c_0^0} + \frac{\sin^2\theta\left(\kappa c_0^0 + c_i^1\right)}{\kappa c_0^0 + c_0^1}\right] v_x(F_i) \\ &+ \sin\theta\cos\theta \sum_{i=1}^{N}\left(\frac{c_i^0}{c_0^0} - \frac{\kappa c_i^0 + c_i^1}{\kappa c_0^0 + c_0^1}\right) v_z(F_i) \end{aligned}, \tag{7}$$

where κ is the local curvature at the intercept point S, c_i^m represents the interpolation coefficient (m=0) and the first order derivative approximation coefficient (m=1) for the associated fictitious points. The particle velocity v_x and v_z at the fictitious points are calculated through interpolation from the wavefields in the surrounding interior cells. Similarly, we are able to calculate v_z(G) defined at the ghost point G.

$$\begin{aligned} v_z(G) = &\sin\theta\cos\theta \sum_{i=1}^{N}\left(\frac{c_i^0}{c_0^0} - \frac{\kappa c_i^0 + c_i^1}{\kappa c_0^0 + c_0^1}\right) v_x(F_i) \\ &- \sum_{i=1}^{N}\left[\frac{\sin^2\theta\, c_i^0}{c_0^0} + \frac{\cos^2\theta\left(\kappa c_i^0 + c_i^1\right)}{\kappa c_0^0 + c_0^1}\right] v_z(F_i) \end{aligned}. \tag{8}$$

When surface topography has large curvature as shown in Figure 4b), some fictitious points (F2, F3) need to be removed because a polynomial approximation is no longer

accurate in representing the wavefields near the surface by using these fictitious points. In practice, the algorithm automatically removes those points with normal distance to the surface boundary larger than 0.3/κ.

Numerical Results

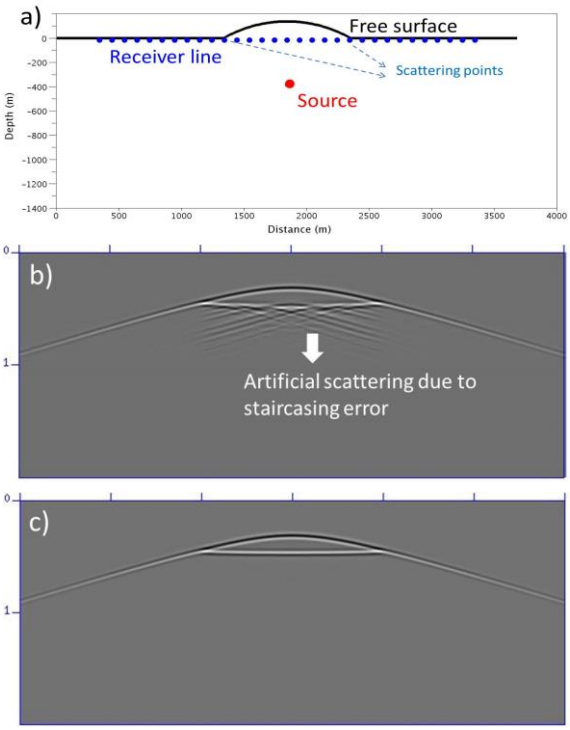

Figure 5: a) simulation geometry; b) conventional finite-difference method simulation result; c) IBFD simulation result (without recursive interplation shceme).

Figure 5a) shows the geometry of the numerical example, where the surface is featuring a curved bump in the middle. Figure 5b) shows the shot gather generated by a conventional finite-difference method, where many artifacts are observed due to the artificial scattering effect caused by the staircasing error. On the other hand, the simulation result produced by the IBFD method (without recursive interpolation scheme) is significantly better with most of the artificial scattering artifacts removed, as shown in Figure 5c).

However, the simulation result in Figure 5c) still has some remaining artifacts (very weak compared with the signal level). To visually boost the artifacts, we re-plotted the Figure 5c) result in Figure 6a) using a different clip parameter. Comparing Figure 6a) and 6b), we note that the artificial scattering effects are further reduced by the recursive interpolation scheme, indicating the IBFD algorithm featuring a recursive interpolation technique is almost immune to staircasing errors.

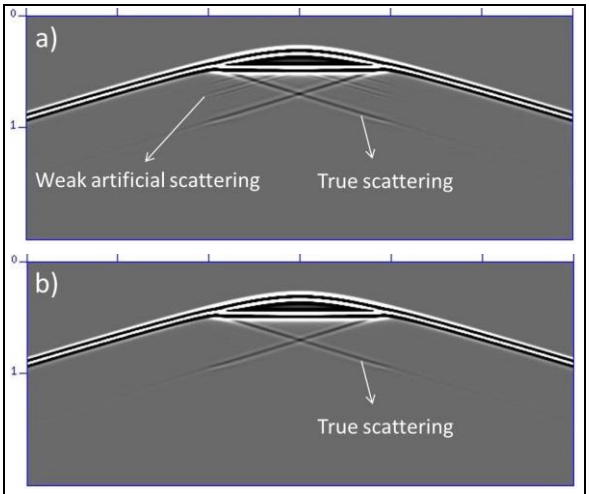

Figure 6: a) IBFD (without recursive interpolation scheme) simulation result; same as Figure 5c) but plotting clip parameter is different to visually boost the artifacts; b) IBFD (with recursive interplation shceme) simulation result.

Conclusions

An accurate and efficient immersed boundary finite-difference method (IBFD) has been developed to model seismic wave propagation with arbitrarily curved surface topography. Unlike FEM, SEM, and some finite-difference algorithms with structured curvilinear body-fitted grids, the IBFD algorithm uses regular Cartesian staggered or collocated grids, which greatly simplifies the mesh generation and related preprocessing procedures. Enforcing the free surface boundary condition at the exact locations through a recursive interpolation technique, IBFD is immune to the notorious staircasing error inevitable in the conventional finite-difference methods. Furthermore, by introducing a local cylindrical or spherical coordinate system, IBFD algorithm is able to precisely capture the effects of local continuity and large curvature on the wave propagation behavior near surface boundary, significantly improving the overall accuracy. Because the ghost zone wavefield extrapolation is only required in the vicinity of the surface, the additional computational cost is negligible even for very high-order finite-difference schemes. Extension to 3D and/or elastic cases is straightforward by replacing the local cylindrical coordinate system with a local spherical coordinate system and modifying the corresponding free surface boundary conditions. Since this algorithm can handle any arbitrarily curved surface topography automatically, it can be a powerful engine for FWI land data processing.

References

Appelö, D. and N. A. Petersson, 2009, A stable finite difference method for the elastic wave equation on complex geometries with free surfaces, Communications in Computational Physics, 5(1), 84-107.

de la Puente, J., M. Ferrer, M. Hanzich, J. E. Castillo, and J. M. Cela, 2014, Mimetic seismic wave modeling including topography on deformed staggered grids, Geophysics, 79(3), T125-T141.

Hestholm, S. and B. Ruud, 1998, 3-D finite-difference elastic wave modeling including surface topography, Geophysics, 63(2), 613-622.

Komatitsch, D. and J. P. Vilotte, 1998, The spectral element method: an efficient tool to simulate the seismic response of 2D and 3D geological structures, Bulletin of the seismological society of America, 88(2), 368-392.

Levander, A. R., 1988, Fourth-order finite-difference P-SV seismograms, Geophysics, 53(11), 1425-1436.

Li, J., Y. Zhang, and M. N. Toksoz, 2010, Frequency-domain finite-difference acoustic modeling with free surface topography using embedded boundary method, Massachusetts Institute of Technology. Earth Resources Laboratory.

Lombard, B., J. Piraux, C. Gélis, and J. Virieux, 2008, Free and smooth boundaries in 2-D finite-difference schemes for transient elastic waves, Geophysical Journal International, 172(1), 252-261.

Min, D. J., C. Shin, R. G. Pratt, and H. S. Yoo, 2003, Weighted-averaging finite-element method for 2D elastic wave equations in the frequency domain, Bulletin of the Seismological Society of America, 93(2), 904-921.

Peskin C. S., 1972, Flow patterns around heart valves: a digital computer method for solving the equations of motion, PhD thesis, Physiol., Albert Einstein Coll. Med., Univ. Microfilms. 378:72–30.

Robertsson, J. O., 1996, A numerical free-surface condition for elastic/viscoelastic finite-difference modeling in the presence of topography, Geophysics, 61(6), 1921-1934.

Zhang, C., and W. W. Symes, 1998, Fourth-order, full-stencil immersed interface method for elastic waves with discontinuous coefficients, SEG Technical Program Expanded Abstracts 1998: pp. 1929-1932. doi:10.1190/1.1820315.